ARTICLE

doi:10.1038/nature10918

Choice-specific sequences in parietal cortex during a virtual-navigation decision task

Christopher D. Harvey[1,3,4]†, Philip Coen[1,4] & David W. Tank[1,2,3,4]

The posterior parietal cortex (PPC) has an important role in many cognitive behaviours; however, the neural circuit dynamics underlying PPC function are not well understood. Here we optically imaged the spatial and temporal activity patterns of neuronal populations in mice performing a PPC-dependent task that combined a perceptual decision and memory-guided navigation in a virtual environment. Individual neurons had transient activation staggered relative to one another in time, forming a sequence of neuronal activation spanning the entire length of a task trial. Distinct sequences of neurons were triggered on trials with opposite behavioural choices and defined divergent, choice-specific trajectories through a state space of neuronal population activity. Cells participating in the different sequences and at distinct time points in the task were anatomically intermixed over microcircuit length scales (<100 micrometres). During working memory decision tasks, the PPC may therefore perform computations through sequence-based circuit dynamics, rather than long-lived stable states, implemented using anatomically intermingled microcircuits.

In real-world tasks, decision-making and working memory often occur in the context of other complex behaviours, including spatial navigation. For example, when driving through a city towards a destination, sensory information defining context and place engages memory and decision circuits to plan turns at upcoming intersections. The PPC is a prime candidate for the neuronal circuitry combining the cognitive processing elements necessary for such tasks. In primates, the PPC is important for perceptual decision-making and categorization[1–3], movement planning[4] and spatial attention[5]. Studies in rats suggest that the PPC is also important for encoding route progression during navigation[6–9]. Using a virtual-reality system for mice[10] and cellular resolution optical imaging methods[11,12], we developed a T-maze-based navigation task combining all these cognitive elements and characterized the neuronal circuit dynamics in the PPC, which have not been studied in this combined behavioural context.

Neuronal activity patterns in the PPC have been studied using microelectrode recordings during spatial attention, working memory and perceptual decision tasks. These studies have commonly found cells with sustained firing rate changes spanning entire task periods (cue, delay, response periods)[2,4,5,13]. For example, cells with persistent activity throughout the delay period of memory-guided saccade/reach tasks have frequently been recorded[14,15]. Also, studies have identified neurons with ramps of increasing firing rate spanning the accumulation of evidence period in a motion perception task[1,2]. Neurons with sustained activity during the same task period often have similar activity time courses, suggesting the presence of classes of cells (for example, delay cells) and implying that the task-dependent neuronal dynamics are low-dimensional. The low-dimensional dynamics can be reproduced in recurrent attractor network models, in which each cell's activity is typically an amplitude-scaled version of a prototypical time series[16–21]. In contrast, recent analysis of prefrontal cortex activity has identified heterogeneous neuronal activity time courses, in which a neuron's activity can be thought of as the sum of a few activity modes[22–24]. In addition, there is growing evidence for sequences of neuronal activation within local circuits, in which each neuron is active for only a fraction of a task period, including during working memory tasks in the prefrontal cortex[25–28] and the hippocampus[29] and during an object construction task in the PPC[30]. Sequences suggest dynamics that are high-dimensional, without the presence of classes of cells with relatively homogeneous activity time courses.

We explored whether PPC dynamics are best described in terms of cell classes or high-dimensional dynamics. During a navigation-based decision task, the dynamics were high-dimensional: neurons were active in choice-specific sequences in which information moves from one neuronal population to another across time in the task; although the neuronal activity patterns could be divided into cue, delay and response groups, sequences were present within each group. Furthermore, exploiting the ability of cellular resolution optical measurements to provide the relative anatomical location of the recorded cells[12,31,32], we found that neurons active during behaviourally distinct task periods and on trials with different behavioural choices were spatially intermixed over microcircuit length scales.

A PPC-dependent navigation-based decision task

Using a virtual-reality system[10], we trained mice to navigate through a virtual T-maze in a task that incorporated both visual discrimination and a memory-guided response (Methods; Fig. 1a). Visual cues present in the initial section of the maze indicated which direction to turn at the T-intersection to receive a water reward (one set of cues to indicate a right turn and a second set for a left turn; Supplementary Fig. 1c). Between the cue section and the T-intersection, mice ran through a delay maze section that was identical on left and right turn trials; visual information about the reward location was thus present only in the cue section. The task resembled traditional delay tasks[14,15,33] in its cue–delay–response structure, but differed in that continuing sensorimotor activity was present throughout the task, including the delay period.

[1]Princeton Neuroscience Institute, Princeton University, Princeton, New Jersey 08544, USA. [2]Bezos Center for Neural Circuit Dynamics, Princeton University, Princeton, New Jersey 08544, USA. [3]Lewis-Sigler Institute for Integrative Genomics, Princeton University, Princeton, New Jersey 08544, USA. [4]Department of Molecular Biology, Princeton University, Princeton, New Jersey 08544, USA. †Present address: Department of Neurobiology, Harvard Medical School, Boston, Massachusetts 02115, USA.

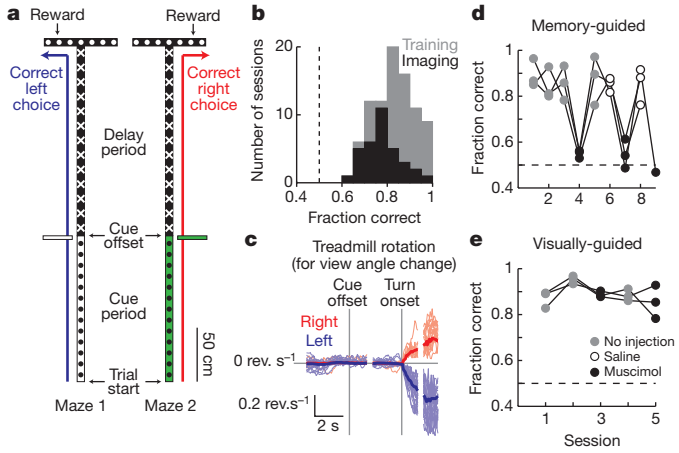

Figure 1 | A PPC-dependent decision task in virtual reality. **a**, Diagram of the two versions of the virtual T-maze that differed only in the cue period and the reward location. Patterns in the diagram reflect the patterns present on the virtual maze walls. **b**, Behavioural performance on individual training (grey) and imaging (black) sessions. **c**, Rotational velocity of the spherical treadmill about the vertical axis for view angle changes on correct right (red) and left (blue) trials, aligned to the cue offset and the turn onset. **d**, Behavioural performance on a memory-guided task from **a** after receiving no injections (grey), saline (open circles) or muscimol (black) bilaterally in the PPC. Connected dots are from individual mice across daily sessions ($n = 3$ mice). **e**, Same as in **d** except for a visually-guided task (Supplementary Fig. 1b; key in **e** applies to **d** also).

Mice performed the task with high levels of accuracy (83 ± 9% correct, $P < 0.0001$ versus 50%, *t*-test; Fig. 1b). Within and across trials, individual mice ran at highly consistent speeds (Supplementary Fig. 2); however, running speeds varied between mice, and the maze position at which mice began rotating the spherical treadmill to make a right or left turn differed across trials (turn onset; Fig. 1c, Supplementary Fig. 3; Methods). To compare behaviourally similar epochs of the task across trials, individual trials were aligned to the time points when the cue was no longer visible (cue offset), the turn onset, and the end of the trial; these alignment points formed the boundaries of cue (trial start to cue offset, 5.1 ± 2.6 s), delay (cue offset to turn onset, 4.2 ± 1.2 s) and turn task periods (turn onset to trial end, 3.0 ± 1.8 s).

Because the location of the mouse PPC has not been characterized, we first performed retrograde and anterograde labelling experiments to locate it anatomically (Methods, Supplementary Fig. 4). We identified a region consistent with the rat and primate PPC based on the set of areas from where it received axonal projections, the areas to which it sent projections, and its location relative to other cortical regions[8,34] (anterior to visual cortex and posterior to somatosensory cortex). We therefore considered this area to be the mouse PPC.

To test if the PPC was required for the behavioural task, we inactivated it using bilateral injections of the $GABA_A$ receptor agonist, muscimol. Muscimol reversibly decreased behavioural performance from high levels of accuracy in control sessions to near chance levels, but did not affect the rate of trials performed (fraction correct; no injections 87 ± 7%, saline 85 ± 5%, muscimol 54 ± 5% $P < 0.0001$ versus no injections, *t*-test: trials per minute; no injections 3.2 ± 0.5, muscimol 3.1 ± 0.3, $P > 0.8$, *t*-test; Fig. 1d). In contrast, PPC inactivation did not significantly affect performance on a visually guided task in which a visual cue was present at the reward site and visible throughout the trial, indicating that the decrease in performance on the memory-guided task was unlikely to be due to a major visual or motor deficit (fraction correct; no injections, 90 ± 5%; muscimol, 87 ± 5%, $P > 0.2$, *t*-test; Fig. 1e, Supplementary Fig. 1b).

Imaging sequences of neuronal activity

We used two-photon microscopy to image layer 2/3 PPC neurons expressing the genetically encoded calcium indicator GCaMP3, which increases in fluorescence intensity in response to action potential firing[35] (Methods). On average, we imaged ~65 cells simultaneously within an area ~300 μm by ~150 μm (range, 37–94 cells). Nearly all imaged cells showed statistically significant Ca^{2+} transients during the behavioural session (96% of cells had >0.2 transients per minute; Methods). Of the cells with high levels of activity (>2 Ca^{2+} transients per minute on average; Supplementary Fig. 5), ~73% had significant increases in their mean fluorescence intensity traces ($\Delta F/F$, averaged across trials) during a specific time in the trial or inter-trial interval (task-modulated cells; Fig. 2, Supplementary Figs 6, 7). These task-modulated cells had Ca^{2+} transients for only short time intervals on individual trials (11 ± 8% of time points in trials with a transient) such that only a small fraction of neurons was active simultaneously (Fig. 2b–e, Supplementary Figs 8, 9a); cells with prolonged activity patterns covering a large fraction of the trial were not observed. The majority (~71%) of task-modulated cells had significantly different levels of activity on correct right and left choice trials (choice-specific cells). Similar choice-specific, task-modulated activity patterns were observed in extracellular electrophysiological recordings (Supplementary Figs 10, 11). Cells were also active on error trials, such that neurons active during the cue period tended to be correlated with the cue identity, and neurons active during the turn period in general were correlated with the behavioural response (Supplementary Fig. 12). Only a small fraction of cells had obvious reward-related signals (~2% of active cells with $P < 0.01$, *t*-test, comparing $\Delta F/F$ values within ~0.6 s after the reward was given on correct trials or missed on error trials).

When the activity patterns of all the choice-specific, task-modulated cells were ordered according to the time profile of their Ca^{2+} transients, the active periods across cells were staggered relative to one another in time, forming a sequence of neuronal activation covering the entire trial length (Fig. 2c, d, Supplementary Fig. 7c). Different sequences of neurons were activated on left and right trials (Fig. 2c, d and absence of activity in Fig. 2d lower plot, Supplementary Fig. 14e). Although these plots of sequences combined cells from different experiments and averaged across trials, similar properties were observed when considering only the cells imaged in a single mouse and on individual trials (Fig. 2c, Supplementary Fig. 13). Sequences were also apparent in the ~29% of task-modulated cells that did not have choice-specific activity; these cells participated in the sequences for both right and left choice trials (Supplementary Fig. 7b). In total, ~73% of the highly active cells participated in sequences. Sequences similar to those during the task were not observed in shuffled versions of the data set, demonstrating that the sequences were not an artefact created by ordering the data (Supplementary Fig. 14a–d).

Because previous studies of the PPC have categorized cells into classes with cue, delay or response period activity[14,15], we examined the activity patterns to see if neurons in the sequence were grouped on the basis of behavioural periods. The distribution of activity times of all cells in the population (calculated for each cell as the centre-of-mass (COM) in time of the mean $\Delta F/F$ during the trial, t_{COM}) had three peaks corresponding to the cue, delay and turn periods, suggesting a possible grouping by behavioural period (Fig. 3a). Consistently, principal component analysis (PCA) of the mean $\Delta F/F$ traces for all cells revealed three intermixed groups, with each group mostly containing cells preferring the same behavioural period (Fig. 3a, b, Supplementary Fig. 15).

Although the population of neurons could be divided into groups, the temporal activity patterns within each individual period were heterogeneous and formed sequences (Fig. 3c). Cells within their preferred period were active for only a fraction of the period (35 ± 16% of time points in preferred periods with a Ca^{2+} transient), with different cells active at different times. Although cells with activity covering a large fraction of the period were occasionally observed (for example, Fig. 2c top panel), these cells were rare (4% of cells with activity lasting for >60% of the period; Supplementary Fig. 9b); the distribution of

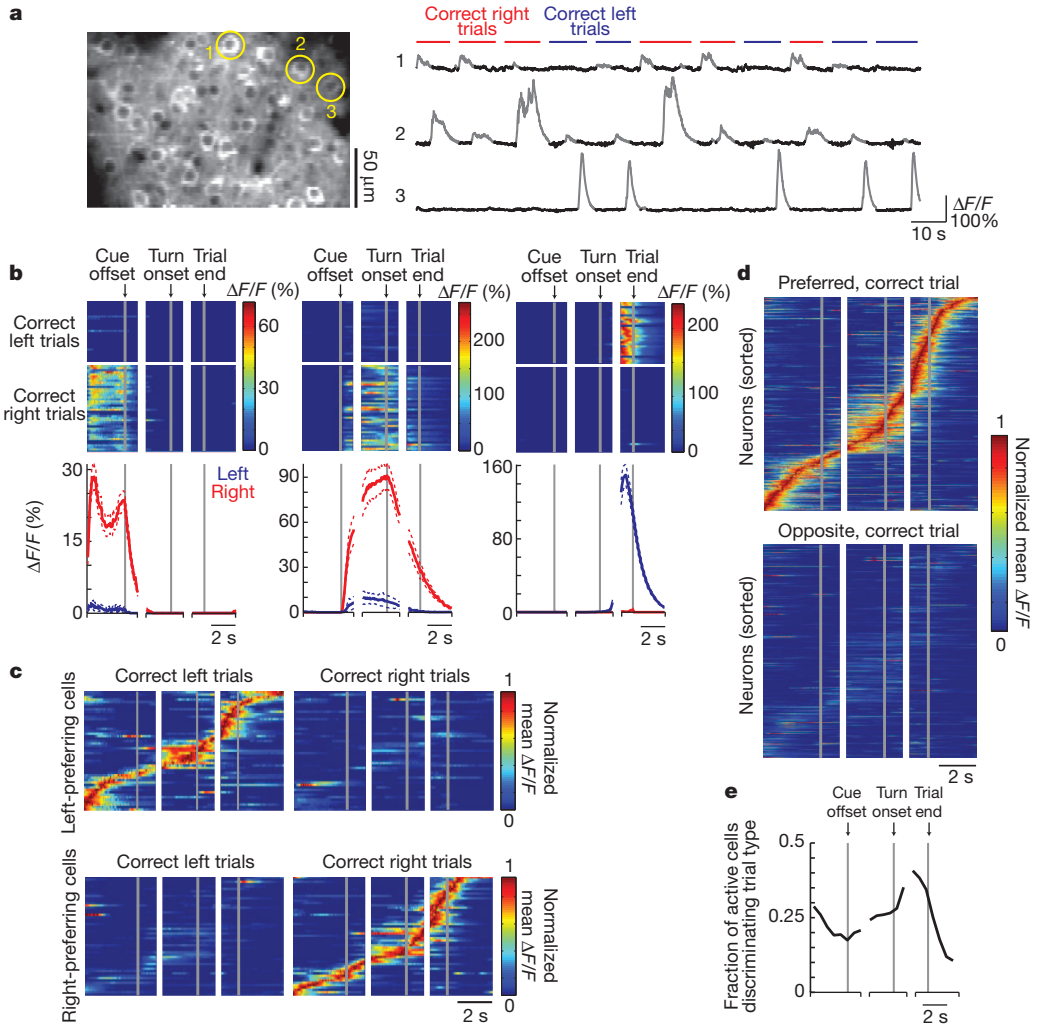

Figure 2 | Imaging PPC neuronal activity during the T-maze task. **a**, Left: example image of GCaMP3-expressing neurons in layer 2/3. Right: example fluorescence intensity traces ($\Delta F/F$; grey portions indicate significant Ca^{2+} transients, Methods) for three example cells from the left panel on correct right (red) and left (blue) trials. **b**, Activity patterns during the task for cells 1–3 from **a**. Top: colour-coded $\Delta F/F$ traces for individual correct left and right choice trials. Each row is a single trial aligned to the cue offset, turn onset and trial end. Bottom: mean $\Delta F/F$ traces for correct right (red) and left (blue) choice trials. Dashed lines indicate mean ± s.e.m. **c**, Normalized mean $\Delta F/F$ traces for all the choice-specific, task-modulated cells (one cell per row) imaged in a single mouse and divided by left-preferring ($n = 51$) and right-preferring ($n = 54$) cells. Traces were normalized to the peak of each cell's mean $\Delta F/F$ trace on preferred trials and sorted by the peak time. Some cells were imaged on different days and in different fields-of-view. **d**, Same as in **c**, except for all mice ($n = 404$ cells from 6 mice) on preferred and opposite trials. **e**, Fraction of active cells with significantly different activity levels on right and left choice trials as a function of trial time.

epoch coverage by an individual neuron's activity was similar during the delay and cue or turn periods ($P > 0.1$, Kolmogorov-Smirnov test). Furthermore, Pearson's correlations between the non-averaged $\Delta F/F$ traces for cell pairs with the same trial-type and behavioural period preferences varied widely, with a large fraction of pairs having low correlation coefficients (Supplementary Fig. 16a). The low correlation coefficients could be due to activity at different times in the period, as expected for sequences, or activity at the same time in the trial except on different trials. However, the probability that both cells in these pairs had Ca^{2+} transients or that both cells did not have transients on the same trial during their preferred epoch was generally high (Supplementary Fig. 16b), suggesting that the diversity primarily resulted from differences in the activity times of cells within trials. Together these data indicate that classes of cells with homogeneous activity patterns were not present. Rather, choice-specific sequences of neurons were activated in all behavioural periods, with a lower density of cells in the sequence at the borders between periods.

To further examine the sequential neuronal activation on individual trials, we calculated correlations between the activity patterns of cells using the non-averaged $\Delta F/F$ time series. Cells that were active at similar time points in the trial on average (measured as the difference in t_{COM} values on correct trials, Δt_{COM}) had, on correct trials and in their preferred behavioural periods, highly correlated $\Delta F/F$ traces and peaks in their cross-correlation at a lag approximately equal to Δt_{COM} (Supplementary Fig. 16d–h); these relationships in the non-averaged $\Delta F/F$ time series provide further evidence for sequential activity on individual trials. Cells that were active at similar times on correct trials were also highly correlated on error trials and in non-preferred periods (Supplementary Fig. 16c–f). Additionally, cells that were sequentially activated during their preferred behavioural period on correct trials were sequentially active with similar lags during error trials and other time points in the task (Supplementary Fig. 16g–i).

The choice-specific activity could result if mice experienced different visual stimuli and running patterns on right and left trials and if PPC activity was modulated by those differences. To examine this, we first performed a multiple regression analysis to determine the potential effects of the parameters defining the mouse's running trajectory on the fluorescence changes during the delay period (Supplementary Table 1). These parameters could not explain the choice-specific

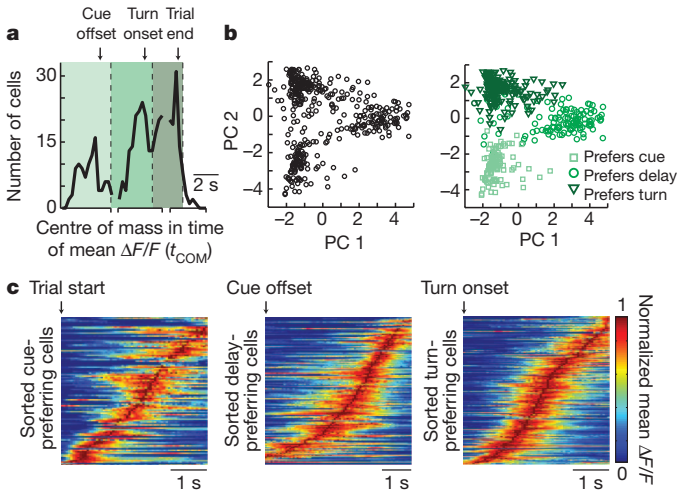

Figure 3 | Neuronal activity in individual behavioural periods. **a**, Histogram of the times of the centre-of-mass of the mean $\Delta F/F$ trace (t_{COM}) for choice-specific, task-modulated cells. Cells were separated into three groups (cue-, delay- and turn-preferring cells; varying shades of green) based on peaks in the distribution. **b**, PCA on the normalized mean $\Delta F/F$ traces for all the choice-specific, task-modulated cells. Left, scores for each cell plotted for the first two principal components (PC 1, 2). Right, cells categorized on the basis of groupings from **a**. $n = 404$ cells. **c**, Sorted normalized mean $\Delta F/F$ traces for cue-preferring ($n = 101$), delay-preferring ($n = 133$) and turn-preferring ($n = 170$) cells, aligned to the trial start, cue offset and turn onset, respectively, on the preferred trial-type.

activity patterns, suggesting that any differences in running trajectories between right and left trials did not trigger the activity we observed. In addition, we performed two sets of experiments to further examine whether the maze visual stimuli alone or the mouse's running patterns triggered PPC activity. In the first experiments, movies of simulated left and right turn runs through the T-maze, which closely approximated real runs, were played to mice that passively viewed the visual scenes (open-loop experiments; Supplementary Fig. 17a, b). In the second experiments, mice were trained on a virtual linear track to perform a simple running back and forth task (run to one end for a reward, turn around, run to the other end for the next reward). The linear track had several visual patterns on the walls, all of which were the same as patterns in portions of the T-maze (Supplementary Fig. 18a, b). The task required similar running and turning behaviours to the T-maze, except that turns were not memory-guided based on visual cues and a delay period, and there was not a two-alternative forced-choice structure. The overall levels of activity during the simulated T-maze runs or during the linear track task were much lower than when mice actively performed the T-maze task (Supplementary Figs 17c, d, 18c, d). Also, only a small fraction of neurons had significant increases in activity at specific locations in the maze, either during the simulated T-maze runs or in the linear track, suggesting that cells were not activated robustly by location-specific visual scenes or running patterns (simulated runs, 1.3% of neurons; linear track, 5.8%; T-maze, 32.3%; Supplementary Figs 17e–k, 18e–k). Together these results suggest that PPC neurons in the T-maze were not activated only by the visual information or by the running patterns of the mouse.

Choice-specific neuronal circuit trajectories

The heterogeneous and sequential neuronal activity patterns during the T-maze task indicated that we should consider the dynamics of the population rather than classes of cells. We therefore analysed the dynamics as a trajectory through a state space of neuronal population activity (neuronal circuit trajectory)[36–38]. At each time point, the activity state of the circuit containing n simultaneously imaged neurons was defined as a point in an n-dimensional space, with each dimension representing the activity ($\Delta F/F$ values) of a single neuron. Different trajectories (visualized using factor analysis for dimensionality reduction) were traversed for trials with different behavioural choices (Fig. 4a, b, Supplementary Fig. 19a). The trajectories for correct right and left choice trials began the trial at similar positions, gradually diverged to reach a peak separation near the time of the behavioural choice, and converged to the starting point in the inter-trial interval (Fig. 4a–d). To quantify the trajectory divergence, we used a classifier based on the distance from an individual trial trajectory to the mean right and left choice trajectories at single time points. It was possible, from the activity of a small population of neurons located in close anatomical proximity (~65 neurons separated by <250 μm), to predict the mouse's choice on single correct trials at better than chance levels during the cue, delay and turn periods (Methods; Fig. 4e, Supplementary Fig. 19b, c). The activity in the PPC can therefore be considered as divergent, choice-specific trajectories through a state space of neuronal population activity.

Trajectories were highly variable on error trials. Some trajectories began close to the correct choice trajectory during the cue period and

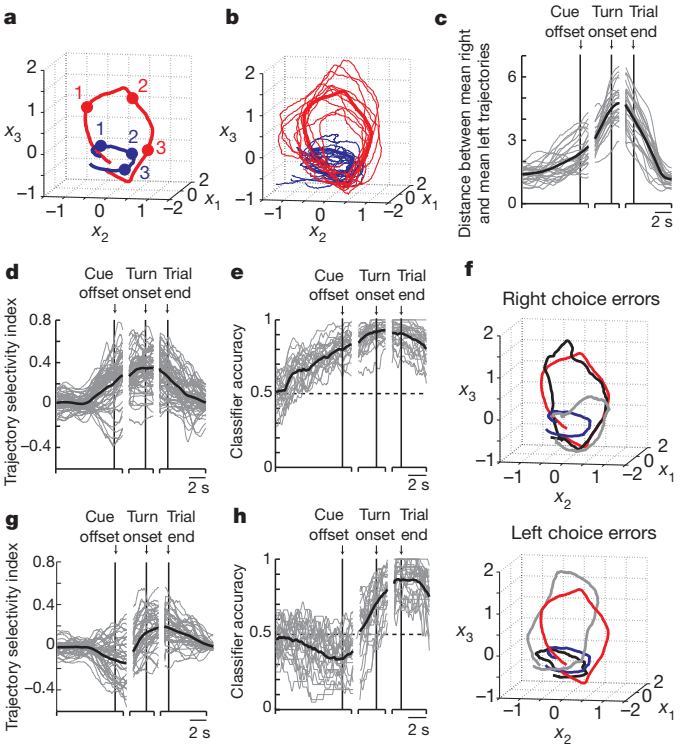

Figure 4 | Neuronal circuit trajectories on correct and error trials. **a**, Time course of mean choice-specific trajectories on correct right (red) and left (blue) choice trials from one session (plotted for the first three common factors). Points labelled 1, 2 and 3 correspond to the mean times of the cue offset, turn onset and trial end, respectively. **b**, Example individual (thin lines) and mean (thick lines) trajectories for correct trials from the session in **a**. **c**, Euclidean distance between the mean trajectories on correct right and left choice trials ($n = 29$ individual sessions, grey). The black line indicates the mean. **d**, Trajectory selectivity index for individual correct trials from a single session, defined on the basis of distances as $(d_{\text{to mean traj, opposite choice}} - d_{\text{to mean traj, same choice}})/(d_{\text{to mean traj, same choice}} + d_{\text{to mean traj, opposite choice}})$. Values close to 1 and −1 indicate that the individual trial trajectory was near the mean trajectory of the same and the opposite behavioural choice, respectively. Mean trajectories were defined using correct trials only. Grey and black lines indicate individual trials and the mean, respectively. **e**, Classification accuracy for determining the behavioural choice of the mouse at different time points in the task during individual sessions (grey, $n = 29$; black, mean). The classifier was based on a distance-dependent classification scheme (see Methods) using correct trials. **f**, Example individual trial trajectories (grey and black) on right choice and left choice errors trials, plotted with the mean trajectories for correct right (red) and left (blue) choice trials. **g**, Same as for **d**, except on error trials. **h**, Same as for **e**, except on error trials.

transitioned towards the error choice trajectory later in the trial; such transitions occurred at a wide range of points in the trial (grey traces in Fig. 4f, Supplementary Fig. 19f). Other trajectories were similar to the error choice trajectory throughout the trial (Fig. 4f, black traces). On average, the error trial trajectories were more similar to the correct choice trajectory during the cue period and closer to the error choice trajectory during the turn period (cue offset; trajectory selectivity index = -0.13 ± 0.22, $P < 0.001$ versus 0, t-test: trial end; trajectory selectivity index = 0.18 ± 0.15, $P < 0.001$ versus 0; Fig. 4g; consistent results based on classification, Fig. 4h). Therefore, individual trajectories transitioned between the mean correct right and left choice trajectories at many time points during trials, but most frequently switched during the delay period.

Anatomical micro-organization of PPC dynamics

To determine how the cells implementing the activity dynamics were anatomically organized, we first examined the neuronal activity patterns to see if cells with different response preferences, such as activity peaks at different times in the trial or different preferences for right and left choice trials, were present in the same regions of the PPC or separated into different areas. Each ~250 μm by ~125 μm area (that is, field-of-view with simultaneously imaged cells) contained both right and left choice-preferring cells of approximately equal numbers and cells with activity peaks at a wide range of times in the trial (Fig. 5a–c, Supplementary Fig. 20). Next, within each imaged area we compared the activities of pairs of neurons as a function of the distance between the neurons' cell bodies. The difference in the trial-type selectivity for cells in a pair did not depend significantly on the distance between cells, indicating that left and right choice-preferring cells were intermixed ($\rho = 0.04$, Spearman's correlation, $P > 0.05$; Fig. 5e). Similarly, Δt_{COM} for a cell pair did not differ with the distance between the cells, indicating that cells active during different periods of the task were intermingled ($\rho = -0.01$, $P > 0.6$; Fig. 5d). However, cells that were separated by less anatomical distance had $\Delta F/F$ traces that were significantly more correlated than cell pairs further apart, but the relationship between the correlation coefficient and distance was weak (all pairs of active cells; $\rho = -0.16$, $P < 0.001$: pairs with the same trial-type and behavioural period preference; $\rho = -0.22$, $P < 0.001$; Fig. 5f). This weak relationship could be due to overlapping fluorescence changes, such as from dendritic signals, or could reflect an actual, weak spatial organization. Regardless, cells with highly different activity patterns were intermixed over short length scales, and an anatomical separation of the response properties we measured was not present.

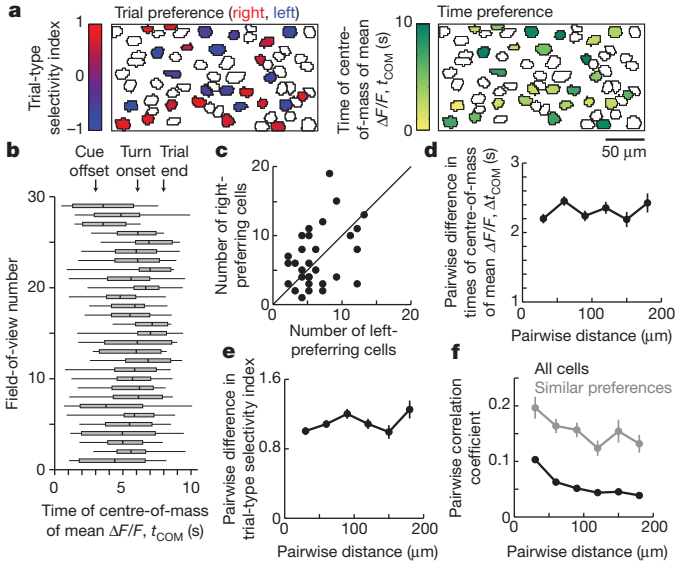

Figure 5 | Anatomical micro-organization in the PPC **a**, Example field-of-view with cells outlined and choice-specific, task-modulated cells coloured. Left, cells' trial-type selectivity, defined as $(\Delta F/F_{\text{right trials}} - \Delta F/F_{\text{left trials}})/(\Delta F/F_{\text{right trials}} + \Delta F/F_{\text{left trials}})$. Values close to 1 (red) and −1 (blue) indicate right and left choice preferences, respectively. Right, cells' time of the centre-of-mass of the mean $\Delta F/F$ trace (t_{COM}). $t_{COM} = 0$ corresponds to ~3 s before the cue offset. **b**, Box plots of t_{COM} values for task-modulated cells in individual fields-of-view (box edges, first and third quartiles; vertical line in the box, median; whiskers, range) **c**, Number of right and left choice-preferring cells in each field-of-view ($n = 29$; unity line is shown). **d**, Difference in t_{COM} as a function of the distance between cells. **e**, Difference in the trial-type selectivity index as a function of the distance between cells. **f**, Pearson's correlation between non-averaged $\Delta F/F$ traces (all time points) for all pairs of active cells (black) and cell pairs with the same trial-type and behavioural period preference (grey) as a function of the cell–cell distance.

Discussion

The choice-specific sequences of PPC neuronal activation we report here add to the growing list of studies that have identified cortical sequences of activity states during working memory tasks[27–30]. Furthermore, because we demonstrated that PPC activity was necessary only for the memory-guided task, the sequences of activation were probably important at least for the memory aspect of the task. Sequence-based dynamics may therefore be a common framework for circuit function during memory and decision tasks, including during navigation behaviours. Such dynamics could potentially be implemented using feedforward architectures[39,40] or liquid state machines[41,42] related to those that have been proposed for working memory.

Our results also offer a way to unite previous work on neural coding in the PPC. Navigation, memory and choice information may be combined in the sequences such that the identity of the active sequence reflects choice-related information for working memory and movement planning[4,5], and that the currently active cell within the sequence reflects spatial or temporal progression through the task[7,43], which were highly correlated in our task (Supplementary Fig. 2). It seems unlikely that PPC neurons only provided location information in a context-dependent manner, like hippocampal place cells[29,44], because unlike place cells PPC neurons did not encode spatial location during a linear track task (Supplementary Fig. 18) or other tasks[6,7].

A possible explanation for heterogeneity and sequences in our experiments versus stereotypy and low-dimensional dynamics, which have been emphasized in previous recordings and models of PPC activity[1,13–18,20,21], is that the PPC adopts different dynamics depending on the demands of the behavioural task. Because traditional delayed saccade tasks, for example, have one spatiotemporal component during the delay period (fixation before making a response), the PPC may adopt sustained activity patterns. In contrast, during tasks that involve many spatial and temporal components, as are common in natural behaviours and during navigation, the PPC may utilize sequences of activation. Alternatively, sequences of activity may be present in the primate PPC during traditional tasks but have yet to be identified, consistent with emerging evidence for heterogeneous temporal response properties[22–24,30]. In addition, different regions or layers of the PPC may have differing activity dynamics[45], or the dynamics of rodent and primate PPC circuits may differ.

Because cells that were active at distinct time points in the task and that participated in different choice-specific sequences were spatially intermingled, our results indicate that functionally distinct subnetworks are anatomically interlaced in the PPC. This extends previous work in sensory cortex, motor cortex and the hippocampus showing spatial intermixing of heterogeneous response properties in cells encoding qualitatively similar types of information (for example, orientation selectivity in visual cortex) or in cells with activity during similar task epochs[12,31,32]. Our findings differ from the predictions of models that have emphasized the spatial clustering of similar response patterns, as in functional columns, and that propose connectivity defined by axonal–dendritic overlap without fine-scale specificity[46,47]. Rather, our results support a model in which microcircuits are formed

by highly specific synaptic connectivity and are composed of neuronal motifs, such as those identified in brain slice recordings in sensory cortices[48,49] and amongst visual cortical neurons with the same orientation selectivity[50]. Our results showing that cell pairs that were sequentially active during their preferred periods on correct trials had similar activity relationships even during error trials and the inter-trial interval suggest the presence of such motifs (Supplementary Fig. 16g-i).

The behavioural task used here did not isolate the decision-making process. We note however that activity trajectories occasionally switched during a trial between the prototypical correct left and right choice trajectories, including frequently on error trials, suggesting that the mouse's decision was not necessarily irreversibly reached immediately after a trial's start (trajectory selectivity switch during the delay period or last 1 s of the cue period; 63% of error trials, 20% of correct trials; Fig. 4d, g, Supplementary Fig. 19e, f). Sequences may therefore play a role in some aspect of decision-related processes, but further experiments will be necessary to assess this possibility.

Our results motivate consideration of a conceptual framework for decision-making and working memory in which sensory information used for the decision activates a neuronal sequence of activity. The sequence begins in a choice-independent state, which could be mediated by neurons that are not choice-specific (Supplementary Fig. 7b), and then moves towards a choice-specific trajectory and away from other trajectories in a manner dependent on the incoming information. A decision is proposed to be reached when the sequence of activity intersects a choice-specific trajectory; different decisions involve intersections with different trajectories. Upon reaching a decision, a working memory can be maintained by continuing along that choice-specific trajectory. Changing decisions would occur through transitions between trajectories, but as time progresses in the task, the state space distance between trajectories increases, in effect creating a larger barrier to change. In this view, decision-making and working memory utilize an ordered progression through a sequence in which information moves from one population of neurons to another over time. The framework we propose is an extension of a point-of-view first considered in describing the dynamics underlying behavioural choices in the leech nervous system[37]. It has some similarities with (and some differences from) drift/diffusion-to-bound, race, and recurrent network models of decision-making implemented as neuronal integrator winner-take-all circuits[2,16]. These models are similar to the trajectory-based view in that different decisions correspond to a divergence in state space surrounding a separatrix. However, these models differ from the sequence framework in that decisions are reached when the activity approaches a choice-specific fixed point with working memory maintained as stable activity at that point. Thus, although these circuits can demonstrate divergent trajectories to reach the fixed points associated with different choices, the trajectories are defined by relatively homogeneous changes in the activity of the population, and the same set of neurons participate in all stages of the decision-making and working memory process.

METHODS SUMMARY

Using a previously described virtual-reality system[10], male C57/BL6 mice were trained using operant conditioning to navigate through a virtual T-maze to receive water rewards. Translation and rotation in the virtual environment were controlled by the mouse's running on a spherical treadmill. Training was performed using shaping implemented as a set of six mazes of increasing task difficulty. Retrograde tracing was performed using fluorescent beads, and anterograde tracing was performed following injections of adeno-associated virus (AAV) containing GFP or GCaMP3. Muscimol injections for PPC inactivation were made bilaterally ~350 μm beneath the dura (50 nl, 1 ng nl^{-1}). Imaging was performed using a custom two-photon microscope incorporated with the virtual-reality system, as described previously[12]. Imaging occurred at 2–6 weeks after injection of AAV2/1-*synapsin-1*-GCaMP3 virus[35]. A complete description of the experimental methods and data analysis is available in the Supplementary Information.

Received 5 December 2011; accepted 2 February 2012.
Published online 14 March 2012.

1. Shadlen, M. N. & Newsome, W. T. Neural basis of a perceptual decision in the parietal cortex (area LIP) of the rhesus monkey. *J. Neurophysiol.* **86,** 1916–1936 (2001).
2. Gold, J. I. & Shadlen, M. N. The neural basis of decision making. *Annu. Rev. Neurosci.* **30,** 535–574 (2007).
3. Freedman, D. J. & Assad, J. A. A proposed common neural mechanism for categorization and perceptual decisions. *Nature Neurosci.* **14,** 143–146 (2011).
4. Andersen, R. A. & Cui, H. Intention, action planning, and decision making in parietal-frontal circuits. *Neuron* **63,** 568–583 (2009).
5. Bisley, J. W. & Goldberg, M. E. Attention, intention, and priority in the parietal lobe. *Annu. Rev. Neurosci.* **33,** 1–21 (2010).
6. McNaughton, B. L. *et al.* Cortical representation of motion during unrestrained spatial navigation in the rat. *Cereb. Cortex* **4,** 27–39 (1994).
7. Nitz, D. A. Tracking route progression in the posterior parietal cortex. *Neuron* **49,** 747–756 (2006).
8. Whitlock, J. R., Sutherland, R. J., Witter, M. P., Moser, M. B. & Moser, E. I. Navigating from hippocampus to parietal cortex. *Proc. Natl Acad. Sci. USA* **105,** 14755–14762 (2008).
9. Calton, J. L. & Taube, J. S. Where am I and how will I get there from here? A role for posterior parietal cortex in the integration of spatial information and route planning. *Neurobiol. Learn. Mem.* **91,** 186–196 (2009).
10. Harvey, C. D., Collman, F., Dombeck, D. A. & Tank, D. W. Intracellular dynamics of hippocampal place cells during virtual navigation. *Nature* **461,** 941–946 (2009).
11. Dombeck, D. A., Khabbaz, A. N., Collman, F., Adelman, T. L. & Tank, D. W. Imaging large-scale neural activity with cellular resolution in awake, mobile mice. *Neuron* **56,** 43–57 (2007).
12. Dombeck, D. A., Harvey, C. D., Tian, L., Looger, L. L. & Tank, D. W. Functional imaging of hippocampal place cells at cellular resolution during virtual navigation. *Nature Neurosci.* **13,** 1433–1440 (2010).
13. Curtis, C. E. & Lee, D. Beyond working memory: the role of persistent activity in decision making. *Trends Cogn. Sci.* **14,** 216–222 (2010).
14. Barash, S., Bracewell, R. M., Fogassi, L., Gnadt, J. W. & Andersen, R. A. Saccade-related activity in the lateral intraparietal area. I. Temporal properties; comparison with area 7a. *J. Neurophysiol.* **66,** 1095–1108 (1991).
15. Chafee, M. V. & Goldman-Rakic, P. S. Matching patterns of activity in primate prefrontal area 8a and parietal area 7ip neurons during a spatial working memory task. *J. Neurophysiol.* **79,** 2919–2940 (1998).
16. Wang, X. J. Decision making in recurrent neuronal circuits. *Neuron* **60,** 215–234 (2008).
17. Wong, K. F. & Wang, X. J. A recurrent network mechanism of time integration in perceptual decisions. *J. Neurosci.* **26,** 1314–1328 (2006).
18. Mazurek, M. E., Roitman, J. D., Ditterich, J. & Shadlen, M. N. A role for neural integrators in perceptual decision making. *Cereb. Cortex* **13,** 1257–1269 (2003).
19. Ganguli, S. *et al.* One-dimensional dynamics of attention and decision making in LIP. *Neuron* **58,** 15–25 (2008).
20. Miller, P., Brody, C. D., Romo, R. & Wang, X. J. A recurrent network model of somatosensory parametric working memory in the prefrontal cortex. *Cereb. Cortex* **13,** 1208–1218 (2003).
21. Machens, C. K., Romo, R. & Brody, C. D. Flexible control of mutual inhibition: a neural model of two-interval discrimination. *Science* **307,** 1121–1124 (2005).
22. Machens, C. K., Romo, R. & Brody, C. D. Functional, but not anatomical, separation of "what" and "when" in prefrontal cortex. *J. Neurosci.* **30,** 350–360 (2010).
23. Jun, J. K. *et al.* Heterogenous population coding of a short-term memory and decision task. *J. Neurosci.* **30,** 916–929 (2010).
24. Singh, R. & Eliasmith, C. Higher-dimensional neurons explain the tuning and dynamics of working memory cells. *J. Neurosci.* **26,** 3667–3678 (2006).
25. Batuev, A. S. Two neuronal systems involved in short-term spatial memory in monkeys. *Acta Neurobiol. Exp. (Warsz.)* **54,** 335–344 (1994).
26. Seidemann, E., Meilijson, I., Abeles, M., Bergman, H. & Vaadia, E. Simultaneously recorded single units in the frontal cortex go through sequences of discrete and stable states in monkeys performing a delayed localization task. *J. Neurosci.* **16,** 752–768 (1996).
27. Baeg, E. H. *et al.* Dynamics of population code for working memory in the prefrontal cortex. *Neuron* **40,** 177–188 (2003).
28. Fujisawa, S., Amarasingham, A., Harrison, M. T. & Buzsaki, G. Behavior-dependent short-term assembly dynamics in the medial prefrontal cortex. *Nature Neurosci.* **11,** 823–833 (2008).
29. Pastalkova, E., Itskov, V., Amarasingham, A. & Buzsaki, G. Internally generated cell assembly sequences in the rat hippocampus. *Science* **321,** 1322–1327 (2008).
30. Crowe, D. A., Averbeck, B. B. & Chafee, M. V. Rapid sequences of population activity patterns dynamically encode task-critical spatial information in parietal cortex. *J. Neurosci.* **30,** 11640–11653 (2010).
31. Ohki, K., Chung, S., Ch'ng, Y. H., Kara, P. & Reid, R. C. Functional imaging with cellular resolution reveals precise micro-architecture in visual cortex. *Nature* **433,** 597–603 (2005).
32. Komiyama, T. *et al.* Learning-related fine-scale specificity imaged in motor cortex circuits of behaving mice. *Nature* **464,** 1182–1186 (2010).
33. Erlich, J. C., Bialek, M. & Brody, C. D. A cortical substrate for memory-guided orienting in the rat. *Neuron* **72,** 330–343 (2011).

34. Corwin, J. V. & Reep, R. L. Rodent posterior parietal cortex as a component of a cortical network mediating directed spatial attention. *Psychobiology* **26,** 87–102 (1998).
35. Tian, L. *et al.* Imaging neural activity in worms, flies and mice with improved GCaMP calcium indicators. *Nature Methods* **6,** 875–881 (2009).
36. Mazor, O. & Laurent, G. Transient dynamics versus fixed points in odor representations by locust antennal lobe projection neurons. *Neuron* **48,** 661–673 (2005).
37. Briggman, K. L., Abarbanel, H. D. & Kristan, W. B. Jr. Optical imaging of neuronal populations during decision-making. *Science* **307,** 896–901 (2005).
38. Churchland, M. M., Yu, B. M., Sahani, M. & Shenoy, K. V. Techniques for extracting single-trial activity patterns from large-scale neural recordings. *Curr. Opin. Neurobiol.* **17,** 609–618 (2007).
39. Goldman, M. S. Memory without feedback in a neural network. *Neuron* **61,** 621–634 (2009).
40. Ganguli, S., Huh, D. & Sompolinsky, H. Memory traces in dynamical systems. *Proc. Natl Acad. Sci. USA* **105,** 18970–18975 (2008).
41. Maass, W., Joshi, P. & Sontag, E. D. Computational aspects of feedback in neural circuits. *PLOS Comput. Biol.* **3,** e165 (2007).
42. Sussillo, D. & Abbott, L. F. Generating coherent patterns of activity from chaotic neural networks. *Neuron* **63,** 544–557 (2009).
43. Leon, M. I. & Shadlen, M. N. Representation of time by neurons in the posterior parietal cortex of the macaque. *Neuron* **38,** 317–327 (2003).
44. Wood, E. R., Dudchenko, P. A., Robitsek, R. J. & Eichenbaum, H. Hippocampal neurons encode information about different types of memory episodes occurring in the same location. *Neuron* **27,** 623–633 (2000).
45. Burke, S. N. *et al.* Differential encoding of behavior and spatial context in deep and superficial layers of the neocortex. *Neuron* **45,** 667–674 (2005).
46. Braitenberg, V. B. & Schuz, A. *Anatomy of the Cortex: Statistics and Geometry* (Springer, 1991).
47. Binzegger, T., Douglas, R. J. & Martin, K. A. A quantitative map of the circuit of cat primary visual cortex. *J. Neurosci.* **24,** 8441–8453 (2004).
48. Yoshimura, Y., Dantzker, J. L. & Callaway, E. M. Excitatory cortical neurons form fine-scale functional networks. *Nature* **433,** 868–873 (2005).
49. Song, S., Sjostrom, P. J., Reigl, M., Nelson, S. & Chklovskii, D. B. Highly nonrandom features of synaptic connectivity in local cortical circuits. *PLoS Biol.* **3,** e68 (2005).
50. Ko, H. *et al.* Functional specificity of local synaptic connections in neocortical networks. *Nature* **473,** 87–91 (2011).

Supplementary Information is linked to the online version of the paper at www.nature.com/nature.

Acknowledgements We thank D. Dombeck for assistance with imaging methods and analysis; C. Domnisoru, M. de Bettencourt, C. Brody and A. Miri for discussions; and M. Goldman, J. Hopfield, D. Aronov, B. Scott and T. Hanks for comments on the manuscript. This work was supported by the NIH (R01-MH083686; RC1-NS068148), a fellowship from the Helen Hay Whitney Foundation (C.D.H.), and a Burroughs Wellcome Fund Career Award at the Scientific Interface (C.D.H.)

Author Contributions C.D.H. performed experiments with assistance from P.C. on the retrograde tracing experiments; D.W.T. implemented the imaging instrumentation; C.D.H. analysed the data with strategy and methods contributions from D.W.T.; C.D.H. and D.W.T. wrote the paper.

Author Information Reprints and permissions information is available at www.nature.com/reprints. The authors declare no competing financial interests. Readers are welcome to comment on the online version of this article at www.nature.com/nature. Correspondence and requests for materials should be addressed to C.D.H. (christopher_harvey@hms.harvard.edu) or D.W.T. (dwtank@princeton.edu).